International Journal of Applied Pharmaceutics

ISSN- 0975-7058 Vol 16, Issue 1, 2024

Original Article

DESIGN AND OPTIMIZATION OF NANO ENCAPSULATED BIO COMPOUNDS OF *ASPARAGUS RACEMOSUS*: BOX BEHNKEN APPROACH

BHARGAVI POSINASETTY[1], SRIVIDYA KOMMINENI[2], RAJASEKHAR KOMARLA KUMARACHARI[3], KISHORE BANDARAPALLE[*], SYED NAZIYA[4], CHANAMBATLA YAMINI[5], DARURI SEEMANTHINI[6]

[1]Senior Clinical Data Manager, Prometrika LLC, Cambridge, MA-02140, USA. Government Dental College and Research Institute, Bellary, Karnataka, India. [2]Process Engineering, Upsher-Smith laboratories, Minnesota-55369, USA. Sri Padmavathi School of Pharmacy, Tiruchanur, Tirupati-517503, Andhra Pradesh. [3]Department of Pharmaceutical Chemistry, Sri Padmavathi School of Pharmacy, Tiruchanoor-517503, Andhra Pradesh, India. [*]Department of Pharmaceutics, Sri Padmavathi School of Pharmacy, Tiruchanoor-517503, Andhra Pradesh, India. [4,5,6]Sri Padmavathi School of Pharmacy, Tiruchanoor-517503, Andhra Pradesh, India

***Corresponding author: Kishore Bandarapalle; [*]Email: kishore.brr89@gmail.com**

Received: 14 Sep 2023, Revised and Accepted: 23 Oct 2023

ABSTRACT

Objective: The current study's objective is to develop and optimize nanoencapsulated bio compounds of *Asparagus racemosus* (BCAR) utilizing the ionic gelation process to target the kidney for antiurolithiatic activity.

Methods: Nanoencapsulated BCAR was prepared employing the ionic gelation method. Box Behnken Design (BBD) 3-factor, 3-level is used to examine the effects of formulation parameters and to enhance the desired responses. Characterization studies include Fourier transform infrared (FTIR), X-ray diffraction (XRD), particle size, zeta potential, scanning electron microscopy (SEM), and transmission electron microscopy (TEM) performed to study the quality of optimized nanoparticles.

Results: Mathematical equations and response surface plots were used to relate the dependent and independent variables. Diagnostic charts were used to show the varied factor-level permutations. The percentages of entrapment efficiency (% EE) and drug release (% DR) used in evaluation studies of optimized bio compounds of BCAR nanoparticles (OBCARNPs) were determined to be 80.67% and 77.4%, respectively. The Fourier transform infrared (FTIR) results showed that chitosan, sodium tripolyphosphate (NaTPP), and BCAR were compatible. Due to chitosan and NaTPP gelation in the case of OBCBANPs, X-ray diffraction (XRD) analyses have acknowledged the crystallinity. The particle size and zeta potential of the optimized formulation, found to be 48.8 nm and 14.1 mV, respectively, indicate the nanoparticles are in the nanorange and possess extreme stability by preventing particle convergence. Scanning Electron Microscopy (SEM) and Transmission Electron Microscopy (TEM) studies reveal that the optimized formulation nanoparticles are spherical in shape, homogeneous, and have little aggregation. The accelerated stability studies showed that the optimized formulation was stable at different temperatures and relative humidity.

Conclusion: The stable, optimized formulation was prepared, evaluated, and characterized. BBD is employed to optimize the formulation by minimizing the number of experimental runs and enhancing the desired responses. The optimized formulation further needs to investigate the *in vivo* studies for antiurolithiatic activity by targeting the kidney.

Keywords: *Asparagus racemosus*, Box-behnken design, Chitosan, Entrapment efficiency, Zeta potential

DOI: https://dx.doi.org/10.22159/ijap.2024v16i1.49377 Journal homepage: https://innovareacademics.in/journals/index.php/ijap

INTRODUCTION

Nanotechnology is a well-established field that encompasses a wide range of applications, including the enhancement of bioavailability and the targeted delivery of medications to specific organs. In this study, we aimed to develop chitosan nanoparticles for encapsulating a selected plant extract containing bioactive compounds. The utilization of low molecular weight chitosan, known for its biocompatibility and biodegradability, was particularly relevant in the creation of polymeric nanoparticles, which are essential for addressing renal calculi formation [1, 2].

The bioactive compounds found in the *Asparagus racemosus* extract exhibit various properties, including antioxidant, diuretic, alkalinizing, and hypocalciuric effects, which are crucial for managing urolithiasis [3, 4]. Megalin receptors in renal tubular epithelial cells are known to bind aminoglycosides. Interestingly, the glucosamine structure shared by aminoglycosides and chitosan polymers led to the discovery that chitosan can effectively act as a ligand for megalin receptors. This characteristic enhances drug accumulation at the desired location within renal tubular epithelial cells, contributing to its significance in this research.

Chitosan plays a pivotal role in guiding bioactive substances to renal cells, thereby enhancing the management of renal calculi, in addition to its biocompatible and biodegradable attributes. This study focuses on the fabrication of chitosan nanoparticles loaded with bioactive constituents from a selected plant extract, aiming to improve medication targeting and bioavailability for the treatment of renal calculi [5-11].

Design of experiments (DOE) has been employed to effectively guide the selection of experimental setups in an optimal manner, reducing process variability. The primary objective of employing DOE is to optimize formulation while minimizing the number of experimental runs and time investment. Among various design strategies, Response Surface Methodology (RSM) is a computational approach that utilizes empirical models based on experimental data. Specifically, the Box-Behnken Design (BBD), a subset of RSM, is frequently employed to evaluate and optimize the main, interactive, and quadratic effects of independent variables or factors. These designs involve three levels for each independent variable. The impacts of different factors can be analyzed using methods such as analysis of variance (ANOVA) and linear regression. Considering this background, the present study focuses on the targeted delivery of bioactive compound-loaded chitosan nanoparticles.

MATERIALS AND METHODS

Chemicals

Analytical grade chemicals obtained from Sigma Aldrich, Hi-media, and Merck India Ltd were used in this study.

Collection and preparation of aqueous extract of *Asparagus racemosus* (BCAR)

The roots of *Asparagus racemosus* were sourced from Sri Srinivasa Ayurvedic Pharmacy, Tirupati. The identification and authentication were conducted by Dr. K. Madhava Chetty, Assistant Professor, Department of Botany, Sri Venkateswara University, Tirupati. A voucher specimen (voucher No: 0698) was submitted to the research center. The roots were dried and coarsely grated. A 100-gram quantity of root powder was macerated with 1L of distilled water for 48 h at room temperature. The resulting extract was concentrated, and the obtained semisolid mass was stored in an airtight container, free from moisture, heat, and air, and labelled as BCAR.

UV spectral analysis of BCAR

The estimation of drug entrapment efficiency in nanoparticles and *in vitro* drug release relied on the calibration curve. UV spectral analysis of BCAR was conducted using a UV-visible spectrophotometer within the range of 200 to 400 nm to determine the maximum absorption wavelength of the selected compounds.

Preparation of bio compounds of *Asparagus racemosus* loaded nanoparticles (BCARNPs)

BCARNPs were formulated by encapsulating BCAR within chitosan nanoparticles through the ionic gelation method. The optimization of BCARNPs was carried out using the BBD.

Box behnken design (BBD)

BBD was employed to investigate the main, interaction, and quadratic effects of variables on formulation efficacy and subsequent optimization. Design Expert software version 11 was used to construct a nonlinear quadratic model. Independent variables, referred to as factors, included the proportions of chitosan, sodium tripolyphosphate, and BCAR. Dependent variables, termed responses, were the percent entrapment efficiency and percent drug release (table 1). Chitosan, sodium tripolyphosphate (NaTPP), and BCAR were denoted as factors A, B, and C, respectively, while percent entrapment efficiency and percent drug release were designated as responses R1 and R2, respectively [12, 13].

Table 1: Independent and dependent variables

Independent variables (Factors)	Dependent variables (Responses)
Polymer (Chitosan)	Percent entrapment efficiency
Cross-linking agent (Sodium tri polyphosphate)	
Drug (BCAR)	Percent drug release

The polynomial equation generated by the BBD was as follows:

The equation representing the relationship between the analyzed response (Y) and the independent variables (A, B, C), along with their interactions and quadratic terms, is expressed as follows:

$$Y=\beta0+\beta1A+\beta2B+\beta3C+\beta4AB+\beta5AC+\beta6BC+\beta7A2+\beta8B2+\beta9C2+E$$

Here,

Y represents the analyzed response,

β0 = intercept,

β1 to β9 are the regression coefficients,

A, B and C = Independent variables (factors), (chitosan, sodium tripolyphosphate and BCAR),

E is error term.

The primary purpose of using surface response plots and two-dimensional contours based on the polynomial equation or model equation is to visualize the relationship between the responses, the components of the mixture, and the numerical factors.

Furthermore, the adequacy of the model was assessed in the study using various techniques. These include residual versus predicted runs, predicted versus actual values, normal residual plots, residual versus actual runs, and residual versus run plots. These assessments will provide insights into the validity and accuracy of the model, aiding in the interpretation of the experimental results.

Evaluation of nanoparticles

Entrapment efficiency

The entrapment efficiency of the drug within the chitosan nanoparticles was determined by quantifying the amount of drug that remained captured. This was achieved by measuring the ratio of the unbound drug present in the supernatant, which is obtained after centrifugation.

After completing the stirring and sonication steps, the preparation was transferred to a centrifuge tube and subjected to centrifugation at 10000 rpm for a duration of 30 min. After centrifugation, carefully collect and measure the total volume of the supernatant, extracting 1 ml. Then, make the necessary dilution of the sample and filter it using a membrane filter. Subsequently, employ a UV spectrophotometer to determine the concentration of BCAR in the sample, utilizing the maximum absorption wavelength (λmax) of 285 nm [14].

By analyzing the entrapment efficiency using this procedure, insights into the proportion of drug successfully encapsulated within the chitosan nanoparticles can be obtained.

$$\text{Free drug (mg)} = \frac{\text{Concentration (µg/ml)} * \text{dilution factor} * \text{volume of supernatant}}{1000}$$

$$\%\ \text{Entrapment efficiency} = \frac{\text{Total amount of drug (mg)} - \text{Free drug(mg)}}{\text{Total amount of drug(mg)}} * 100$$

***In vitro* drug release**

In vitro drug release analysis was conducted to investigate the release rates of BCAR from the corresponding nanoparticle system. For this purpose, the dialysis bag method was employed, utilizing a dialysis membrane with a molecular weight cut-off of approximately 12000-14000 Da (pore diameter; Himedia, Mumbai). The dialysis membrane was pre-soaked in normal saline overnight to facilitate the opening of pores. Subsequently, sealed nanoparticles containing an equivalent weight of 500 mg BCAR were placed within the dialysis membrane [15].

At each specified interval, a 1 ml aliquot was withdrawn through a sample collector to quantify the amount of drug that had diffused through the dialysis membrane. This withdrawn sample was then replenished with a fresh buffer solution to maintain a consistent dissolution medium volume. The collected samples were diluted to a total volume of 10 ml using a volumetric flask and analyzed at a wavelength of 285 nm using a UV-visible spectrophotometer to quantify the concentration of BCAR.

By tracking the drug release over time using this methodology, insights into the release kinetics and behavior of BCAR from the nanoparticles can be obtained.

$$\text{Amount of drug released (mg)} = \frac{\text{Concentration (µg/ml)} * \text{dilution factor} * \text{volume of supernatant}}{1000}$$

$$\text{Drug release \%} = \frac{\text{Amount of drug release (mg)}}{\text{Total amount of drug(mg)}} * 100$$

Release kinetics

To comprehend the drug release mechanism from the formulation, the *in vitro* drug release data was fitted to different kinetic models. These models include zero-order, first-order, Higuchi, Hixson-Crowell, and Korsmeyer-Peppas models [16, 17].

Optimization

Numerical optimization was carried out using a desirability index set close to 1 in order to select the optimal set of variables that yielded the desired outcome. The optimization priorities encompassed maximizing the percent entrapment efficiency and the percent drug release. Furthermore, a comparison between the mean experimental results and the predicted values, along with the determination of percent error, was performed to validate the optimization process. The experiment was replicated in triplicate to ensure the robustness of the optimized conditions [18].

Characterization of optimized nanoparticles

Fourier transform infrared (FTIR) studies

Spectral FTIR analyses were conducted using the pressed pellet technique. In this procedure, a 1:100 ratio of sample to potassium bromide was employed. The resulting mixture was compressed into a thin, transparent disc using a hydraulic press under a vacuum pressure of 800 mPa. The FTIR spectrophotometer was utilized to scan the samples within the range of 4000-400 cm-1 to ascertain the molecular environment of the samples. Samples subjected to FTIR analysis included BCAR, chitosan, sodium tripolyphosphate, and the optimized BCAR formulation. The obtained IR spectrum of the optimized formulation was compared with the FTIR spectra of pure extract and excipients to identify any interactions [19].

X-ray diffraction (XRD) studies

Powder X-ray diffraction patterns of BCAR, chitosan, blank nanoparticles, and optimized nanoparticles were obtained using an Xpert-proanalytical diffractometer (Shimadzu-6005). The samples were exposed to Cu-Kα radiation at 56 kV and 182 mA across the 2θ range of 0 °C to 80 °C.

Particle size measurement

Dynamic light scattering (DLS) was used to analyze the size of optimized nanoparticles. Samples were placed in square glass cuvettes, and after dilution with excess water, the movement of charged colloidal particles under the influence of an applied electric field was observed.

Zeta potential measurement

Zeta potential for the optimized nanoparticles was determined using the DLS technique on a Nanopartica (HORIBA, SZ-100) compact scattering spectrometer. Samples were placed in clear disposable zeta cells, and the results were recorded.

Scanning electron microscopy (SEM)

The structural and morphological characteristics of the optimized nanoparticle formulation were examined using a scanning electron microscope (HR-SEM), specifically Hitachi's SU6600, operating at an accelerating voltage of 30 kV and magnifications ranging from 10X to 600,000X.

Transmission electron microscopy (TEM)

The surface morphology and size of the nanoparticles were analyzed using transmission electron microscopy (JEOL, JEM-1010) with an accelerating voltage of 80 kV. A drop of aqueous optimized nanoparticles was placed on a carbon-coated copper TEM grid, dried, and kept under vacuum before loading onto a specimen holder. The particle size and surface morphology were evaluated using Image J 1.45s software [20].

Stability studies

The stability of the optimized nanoparticles was assessed at various conditions, including 25 °C/60% RH, 45 °C/65% RH, and 60 °C/75% RH, as per the ICH guidelines. The study period spanned 15, 30, 60, and 90 d. Physical appearance and *in vitro* drug release were examined at each interval.

RESULTS AND DISCUSSION

UV spectral analysis of BCAR

BCAR solution was scanned within the range of 200 to 400 nm, revealing an absorption maximum at 285 nm, which was used for subsequent studies as shown in fig. 1.

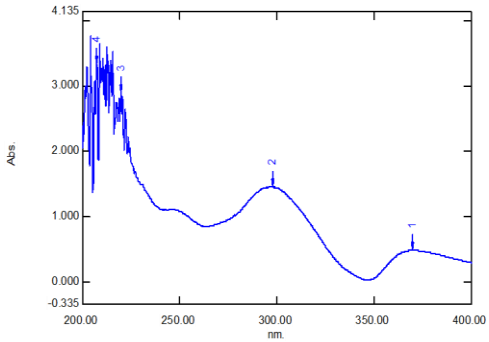

Fig. 1: UV-Vis absorption spectra of BCAR

Box behnken experimental design (BBD)

BBD was employed to optimize BCARNPs using Design Expert software version 11. This design generated 17 formulation runs with five center points involving low, middle, and high levels of formulation factors (as detailed in table 2). The statistical model's validity was evaluated through ANOVA.

Table 2: Independent variables, levels and range used in BBD for BCARNPs

Levels						
Independent variables	**Low**		**Middle**		**High**	
	Coded	**Actual**	**Coded**	**Actual**	**Coded**	**Actual**
A: Amount of Polymer	-1	1	0	1.5	+1	2
B: Amount of Cross linker	-1	0.75	0	1.25	+1	1.75
C: Amount of Drug	-1	300	0	375	+1	450

Polymer: chitosan (g), Cross linker: NaTPP (g), Drug: BCAR (mg)

For the preparation of BCBANPs, the above formulation table 2 lists the coded and actual independent factors (amount of polymer, cross-linker, and drug) with desired responses, including % EE (R1) and % DR (R2).

In the current study, the optimization was established using a BBD with three factors and three levels. Chitosan, NaTPP, and BCAR are the three variables that were selected. %EE and %DR are the two dependent variables specified for the research. Trials at various extreme levels were conducted in order to establish the levels of high, middle, and low for each factor. Depending on the results of the trails, the low (-1), middle (0), and high (+1) levels for BCARNPs are 1g, 1.5g, and 2g for chitosan, 0.75g, 1.25g, and 1.75g for NaTPP, and 300 mg, 375 mg, and 450 mg for BCAR, as displayed in table 2.

By inputting the data regarding the levels of factors, design expert software version 11 is employed to generate the required experimental runs. With five centre points in BCARNPs, the design expert program version 11 generates a total of 17 trial runs. At the central point, all variables are in the middle.

Table 3: Amount of each independent variable and observed responses of 17 formulations of BCAR

Factors responses[a]					
Runs	**A**	**B**	**C**	**R1 (%)**	**R2 (%)**
1	1.5	1.25	375	83.2±0.86	78.5±3.20
2	2	1.25	450	84.3±0.17	80.7±2.89
3	1	0.75	375	79.6±0.54	70.6±2.34
4	1.5	1.25	375	83.2±0.46	78.6±2.17
5	1	1.25	300	75.57±0.33	72.3±2.37
6	1.5	1.25	375	83.1±0.82	79.3±2.81
7	1.5	1.25	375	82.9±0.28	78.2±2.19
8	1.5	0.75	300	76.5±0.59	71.5±2.08
9	1.5	1.75	450	84.54±0.67	82.4±3.24
10	1	1.25	450	79.9±0.39	74.8±2.87
11	2	1.25	300	80.47±0.71	78.6±2.93
12	1.5	1.25	375	84±0.96	78.5±2.07
13	2	0.75	375	75.7±1.34	81.6±3.12
14	1	1.75	375	78.7±0.45	82.4±2.91
15	2	1.75	375	88.5±0.73	86.6±3.01
16	1.5	1.75	300	78.59±0.26	81.5±2.93
17	1.5	0.75	450	76.5±1.16	78.3±3.09

A: Amount of Chitosan (g), B: Amount of Sodium Tri Polyphosphate (g), C: BCAR (mg), R1: Percent entrapment efficiency (% EE), R2: Percent drug release (% DR). Results mentioned are mean±SD; n=3.

Polynomial equation for BCARNPs

The quality characteristics of BCARNPs were evaluated using the Box-Behnken Design, which produced a polynomial equation relating responses (percent entrapment efficiency, % EE, and percent drug release, % DR) to the independent variables. Actual response values were obtained by substituting factor values into the equation.

$$\%\ EE = 83.28+1.90\ A+2.75\ B+1.76\ C+3.42\ AB-0.1250\ AC+1.49\ BC-0.8138\ A2-1.84\ B2-2.41\ C2 \quad (5.1)$$

$$\%\ DR = 78.62+3.42\ A+3.86\ B+1.54\ C-1.70\ AB-0.1\ AC-1.47\ BC-0.0725\ A2+1.75\ B2-1.95\ C2. \quad (5.2)$$

Fitting of data in the selected model

Upon fitting the collected dependent variable data into various models, the quadratic model was determined to be the most suitable fit for both % EE and % DR. Within the polynomial regression equation, a positive sign indicates a synergistic effect on optimization, while a negative sign signifies an antagonistic effect.

Effects of variables on responses

The independent variables A (chitosan), B (sodium tripolyphosphate), and C (BACAR) exhibited statistically significant influences on both % EE (R1) and % DR (R2), as stated in table 4. The sign and magnitude of the regression coefficients signify the nature and extent of their impact on the desired response. All variables possess positive regression coefficients, indicating a synergistic effect on both % EE and % DR. NaTPP had a significant impact on % EE, whereas chitosan and NaTPP showed notable effects on % DR.

Interaction effects of variables on responses

The interaction effects of variables reveal how a combination of variables simultaneously affects responses. The AB (chitosan and NaTPP) and BC (NaTPP and BACAR) interaction effects showed significant consequences on % EE and % DR, as indicated in table 4. AB and BC exhibited positive effects on % EE, suggesting a synergistic effect, while BC displayed a negative effect on % DR, implying an antagonistic impact. These interaction effects show that as the concentrations of specific variables increase together, the desired responses may either increase (synergistic) or decrease (antagonistic).

Table 4: Regression coefficients of actual values and model adequacies for responses of BCAR

	Responses	
	R1	**R2**
A	+1.90	+3.42
P value	<0.0001*	<0.0001*
B	+2.75	+3.86
P value	<0.0001*	<0.0001*
C	+1.76	+1.54
P value	0.0001*	0.0006*
AB	+3.42	-1.70
P value	<0.0001*	0.0026*
AC	-0.1250	-0.10
P value	0.7206	0.7966
BC	+1.49	-1.47
P value	0.0030*	0.0055*
A^2	-0.8138	-0.0725
P value	0.0418*	0.8478
B^2	-1.84	+1.75
P value	0.0008*	0.0019*
C^2	-2.41	-1.95
P value	0.0002*	0.0011*
lack of fit F value	4.61	6.46
lack of fit p-value	0.0870	0.0516
Model F value	53.16	55.74
Model p-value	<0.0001	<0.0001
Residual R square	0.9856	0.9862
Adjusted R square	0.9670	0.9685
Pred R-Squared	0.8160	0.8138
C. V. %	0.8299	0.9516

*Represents a significant effect on responses. R1: Percent entrapment efficiency, R2: Percent drug release

Quadratic effects of variables on responses

The quadratic effects of variables involve the influence of their square terms on the responses. Quadratic variables A2, B2, and C2 significantly affected % EE, while B2 and C2 significantly affected % DR. Quadratic variables had a negative effect on % EE, while B2 had a positive effect and C2 had a negative effect on % DR, as shown in table 4. The high value of the regression coefficient for C2 on % EE suggests that increasing BACAR concentration leads to a reduction in % EE due to increased free drug concentration. Quadratic terms B2 and C2 had both synergistic and antagonistic influences on % DR [21].

The effects of each independent variable on the responses were further explored using three-dimensional response surface graphs fig. 2 (A-F). These graphs provided insights into how variations in each variable influenced % EE and % DR.

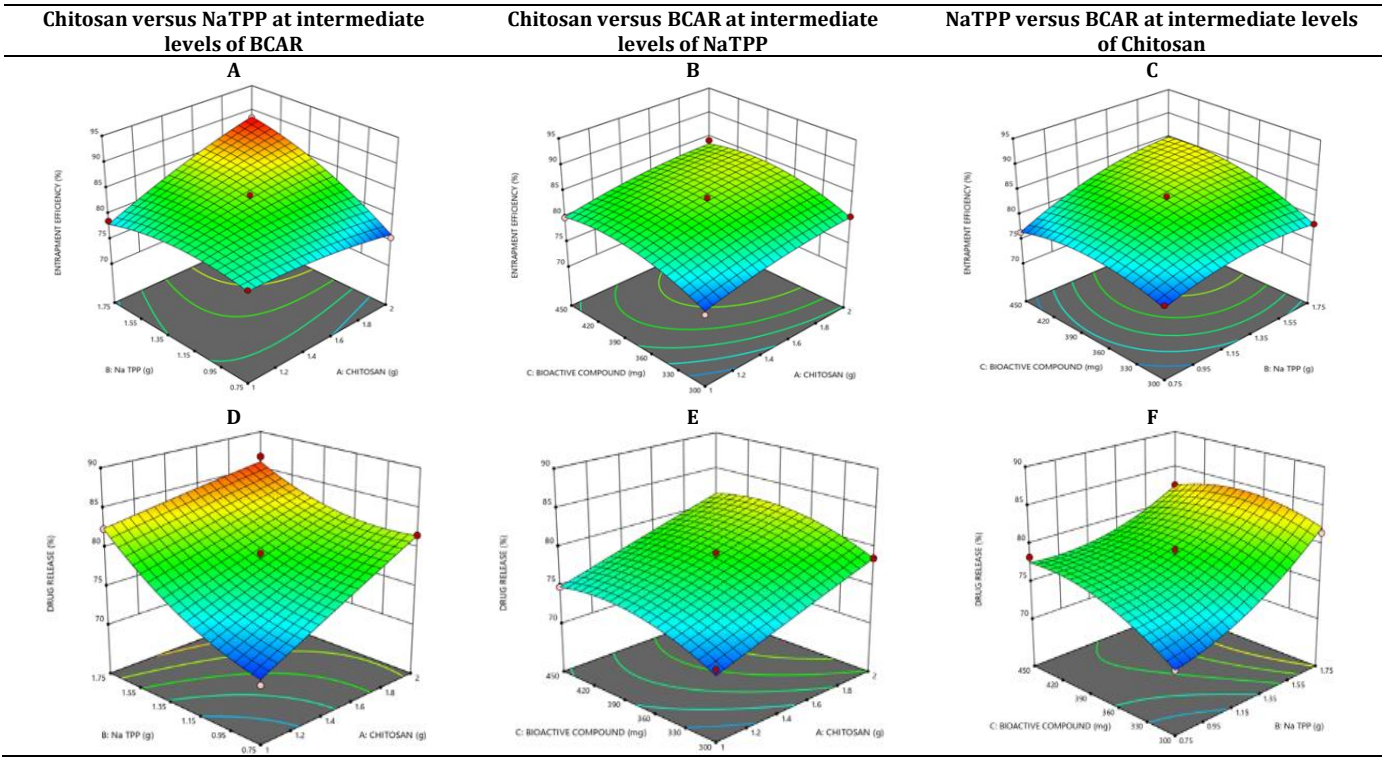

Fig. 2 (A-F): 3D Response surface plots of BCAR, R1: A-C, R2: D-F at different levels of A, B and C

Diagnostic and contour plots of responses

The halfway normal plots in fig. 3 indicated that if the residual values align relatively closely or follow a straight line with the S-shaped curve, the model is significant [22].

Residual vs. Predicted data plots in fig. 4 showed a random dispersion of points within the red lines, indicating the absence of outliers and confirming the model's adequacy [23].

Predicted vs. Actual plots in fig. 5 demonstrated that predicted and experimental responses closely aligned with a straight line, affirming a linear relationship between variables and responses [24].

Residual vs. Run plots in fig. 6 showed a random scatter of points within the red lines, indicating a linear correlation between variables and responses [25].

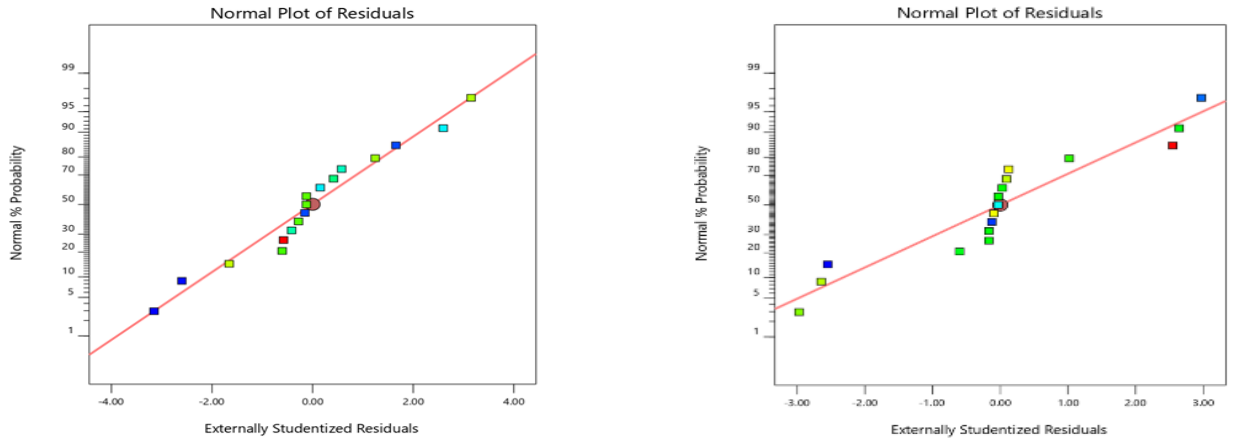

% Entrapment efficiency **% Drug release**

Fig. 3: Externally studentized/halfway plots of responses of BCARNPs, R1 and R2

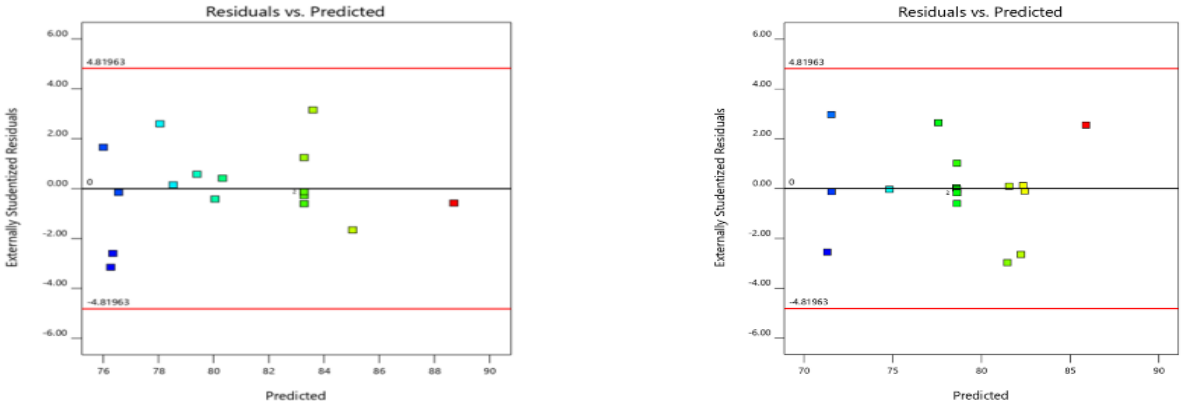

% Entrapment efficiency **% Drug release**

Fig. 4: Residual vs predicted plots of responses of BCARNPs, R1 and R2

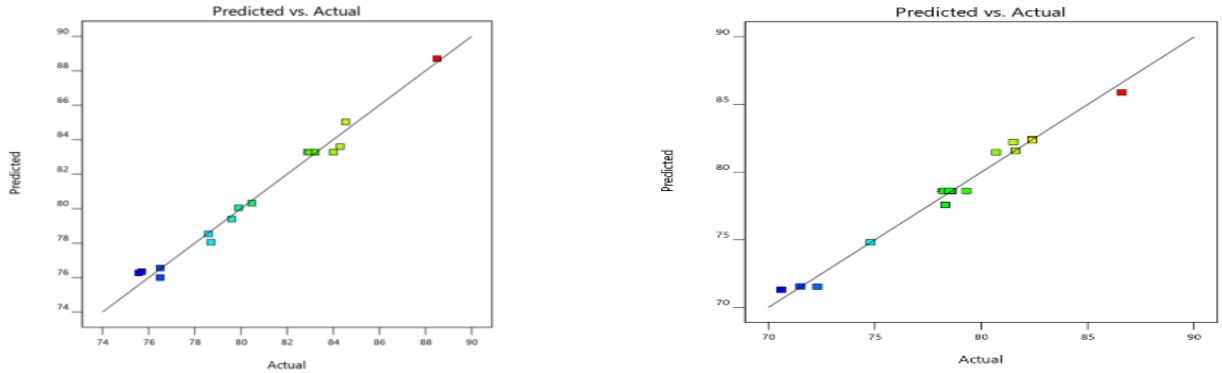

% Entrapment efficiency **% Drug release**

Fig. 5: Predicted vs actual plots of responses of BCARNPs, R1 and R2

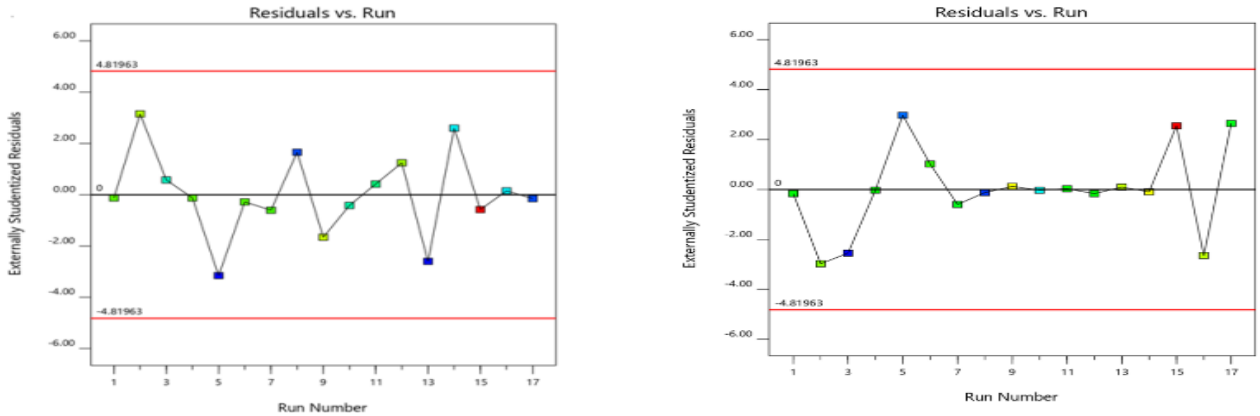

% Entrapment efficiency **% Drug release**

Fig. 6: Residual vs run plots of responses of BCARNPs, R1 and R2

Two-dimensional contour plots in fig. 7 provided insights into the effect of two factors or their combinations on responses, with darker regions indicating higher levels of specific responses.

Percent entrapment efficiency (% EE)

The % EE for the 17 experimental runs ranged from 75.57±0.33 % (R5) to 88.5±0.73 % (R15) portrayed in fig. 8.

***In vitro* dissolution studies of BCARNPs**

The dissolution study of BCAR-loaded chitosan nanoparticles was conducted using the dialysis bag method.

The drug release behavior of BCAR entrapped within chitosan nanoparticles was investigated using an *in vitro* dialysis bag method with phosphate buffer saline pH 7.4 as the dissolution medium for 24 h. The results obtained at various time intervals indicated an initial burst release followed by sustained release. The initial burst release ranged from 7.6% to 21.3% at 30 min for formulations R3 and R15, respectively. Over the course of 24 h, the cumulative drug release from the nanoparticles ranged from 70.6% to 86.6%, with formulations R3 and R15 showing the lowest and highest drug release, respectively, depicted in fig. 9 to 12.

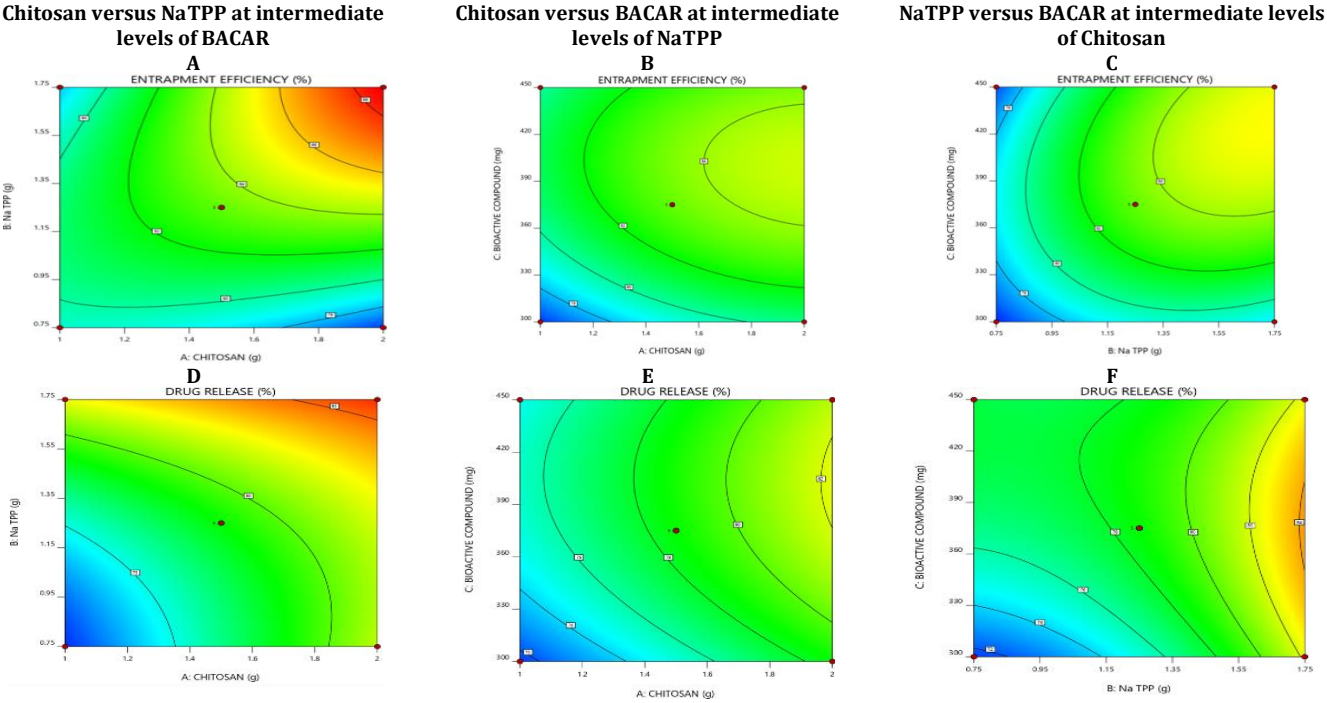

Fig. 7: 2-D plots of responses of BCARNPs, R1 and R2

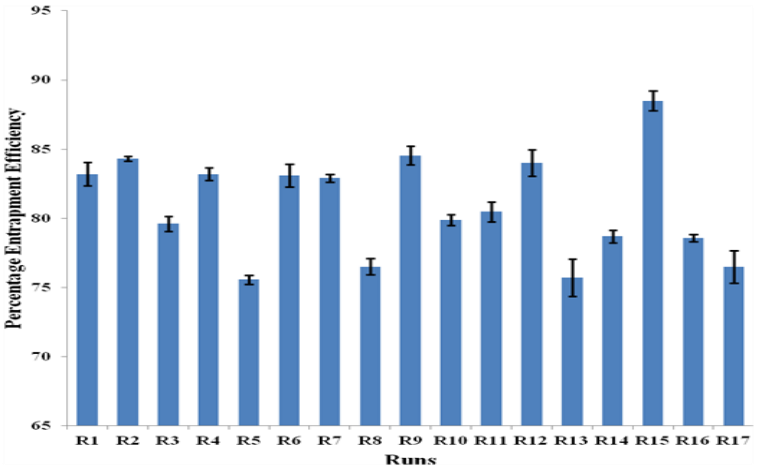

Fig. 8: % EE of BCARNPs runs, results mentioned are mean±SD; n=3

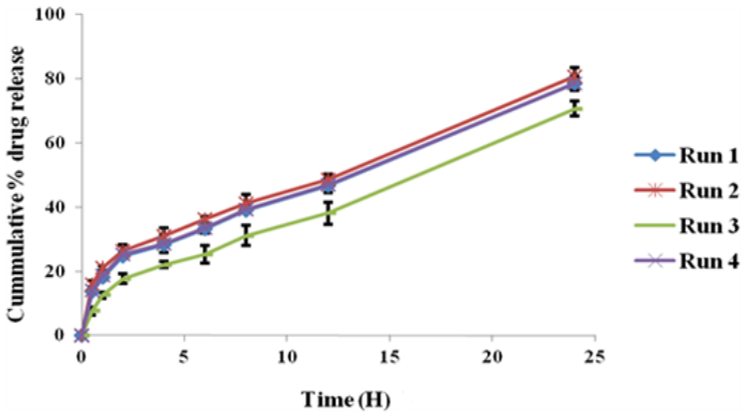

Fig. 9: *In vitro* dissolution profiles of runs 1-4 formulations of BCARNPs, results mentioned are mean±SD; n=3

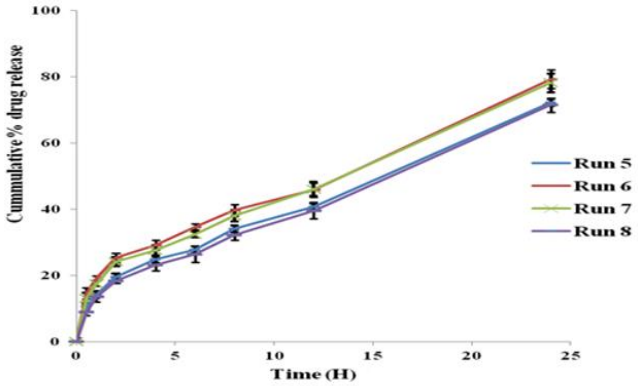

Fig. 10: *In vitro* dissolution profiles of runs 5-8 formulations of BCARNPs, results mentioned are mean±SD; n=3

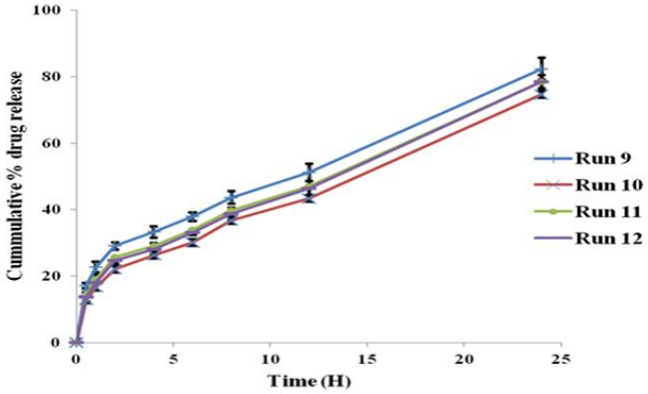

Fig. 11: *In vitro* dissolution profiles of runs 9-12 formulations of BCARNPs, Results mentioned are mean±SD; n=3

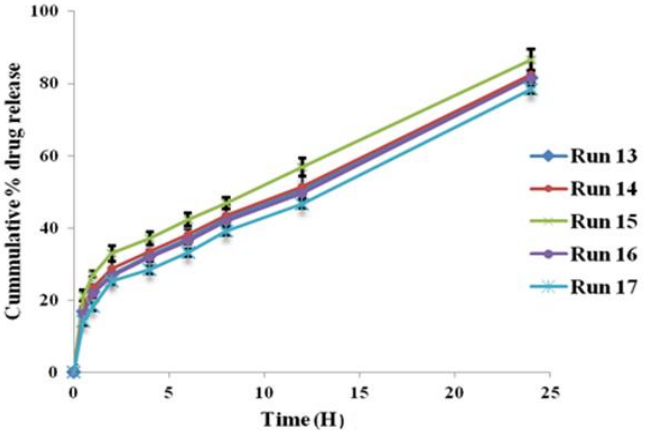

Fig. 12: *In vitro* dissolution profiles of runs 13-17 formulations of BCARNPs, results mentioned are mean±SD; n=3

The variation in drug release can be attributed to differences in the entrapment efficiency of the formulations. The rate of drug release is generally proportional to the amount of drug entrapped in the nanoparticles. Formulations with higher entrapment efficiency tend to exhibit a faster initial release due to the higher concentration gradient, followed by sustained release. This explains why formulation R15, with the highest entrapment efficiency of 88.5%, exhibited the highest drug release, while formulation R3, with an entrapment efficiency of 79.6%, showed lower drug release.

Mathematical model fitting of obtained drug release data for BCARNPs

The drug release profiles obtained from all 17 runs of BACAR-loaded chitosan nanoparticles were fitted to various drug release kinetic models, including zero-order, first-order, Higuchi, Hixson Crowell, and Korsmeyer Peppas models. The correlation coefficient values (r) were found to be highest for the Higuchi and Korsmeyer Peppas models outlined in table 5. The high r values for these models indicated that the drug release mechanism involves diffusion into the dissolution medium through the swelling of the formulation. The n values of the Korsmeyer Peppas model ranged from 0.3177 to 0.4784, suggesting that the drug release mechanism from the nanoparticles is Fickian diffusion, where diffusion rate is influenced by surface area, concentration gradient and membrane thickness.

Optimization of BCARNPs

The optimization of BACAR-loaded chitosan nanoparticles was performed using numerical optimization techniques to maximize the

percent entrapment efficiency and percent drug release. The optimized formulation was determined to have chitosan 1.411 g, sodium tripolyphosphate 1.234 g, and BACAR 350 mg, with predicted responses of 82% for % EE and 77.13% for % DR. Experimental responses were 80.67% for % EE and 77.40% for % DR, as shown in table 6. The optimization process was validated by comparing experimental and predicted responses, resulting in percent errors ranging from-5.26% to 3.45%.

Table 5: Release kinetics of BCARNPs

Runs	Zero order (r)	First order (r)	Higuchi (r)	Hixson crowell (r)	Korsmeyer peppas	
					(r)	(n)
R1	0.8305	0.9708	0.9861	0.9472	0.9839	0.4063
R2	0.7794	0.9637	0.9825	0.9327	0.9820	0.3736
R3	0.9136	0.9737	0.9720	0.9654	0.9824	0.4784
R4	0.8028	0.9646	0.9827	0.9364	0.9792	0.3858
R5	0.8807	0.9741	0.9831	0.9580	0.9832	0.4347
R6	0.8066	0.9651	0.9829	0.9383	0.9817	0.3862
R7	0.8391	0.9715	0.9854	0.9494	0.9826	0.4064
R8	0.8997	0.9771	0.9813	0.9644	0.9851	0.4608
R9	0.7303	0.9585	0.9797	0.9191	0.9825	0.3552
R10	0.8382	0.9669	0.9835	0.9434	0.9790	0.3964
R11	0.7982	0.9638	0.9835	0.9346	0.9833	0.3850
R12	0.8280	0.9692	0.9842	0.9457	0.9814	0.3970
R13	0.7529	0.9590	0.9787	0.9242	0.9793	0.3578
R14	0.7134	0.9552	0.9769	0.9132	0.9806	0.3462
R15	0.6255	0.9526	0.9661	0.8991	0.9774	0.3177
R16	0.7718	0.9643	0.9829	0.9230	0.9820	0.3693
R17	0.8203	0.9684	0.9841	009433	0.9798	0.3910

Results were mentioned as the number of experiments (n=3)

Table 6: Predicted and experimental responses of numerical optimization BCARNPs

Factors	Predicted values	Actual operable optimal conditions	Responses	Predicted responses	Experimental responses
Chitosan	1.411 g	1.41 g	% EE	82 %	80.67±1.43 %
NaTPP	1.235 g	1.24 g	% DR	77.13 %	77.40±2.77%
BACAR	350 mg	350 mg			

Results were mentioned as mean±SD; n=3

Mathematical model fitting of obtained drug release data for OBCARNPs

The drug release profiles from the optimized formulation (OBACARNPs) were fitted to various drug release kinetic models, including zero-order, first-order, Higuchi, Hixson Crowell, and Korsmeyer Peppas models. The highest correlation coefficient values (r) were observed for the Higuchi and Korsmeyer Peppas models, indicating that the drug release mechanism from the optimized formulation involves diffusion into the dissolution medium through swelling. The n value of the Korsmeyer Peppas model was found to be 0.3703, indicating Fickian diffusion as the predominant release mechanism stated in table 7 and fig. 13.

Characterization studies

FTIR studies

The FTIR spectra of the BACAR mixture with chitosan and sodium tripolyphosphate showed peaks corresponding to various functional groups, confirming the compatibility of BACAR with the other components in fig. 14-17.

Table 7: Release kinetics of OBCARNPs

Run	Zero order (r)	First order (r)	Higuchi (r)	Hixson Crowell (r)	Korsmeyer Peppas	
					(r)	(n)
OBACARNPs	0.7803	0.9593	0.9822	0.9259	0.9785	0.3703

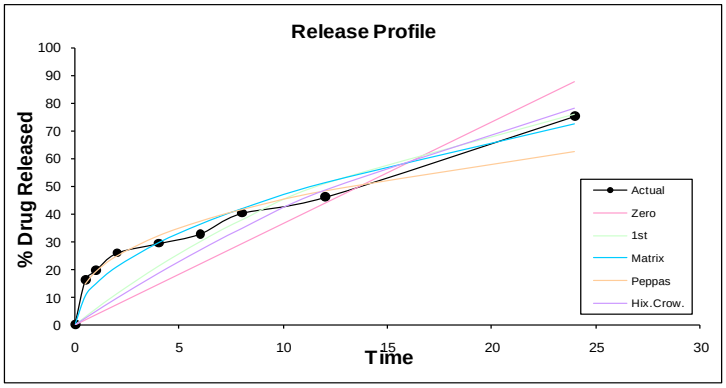

Fig. 13: Release kinetics of OBCARNPs

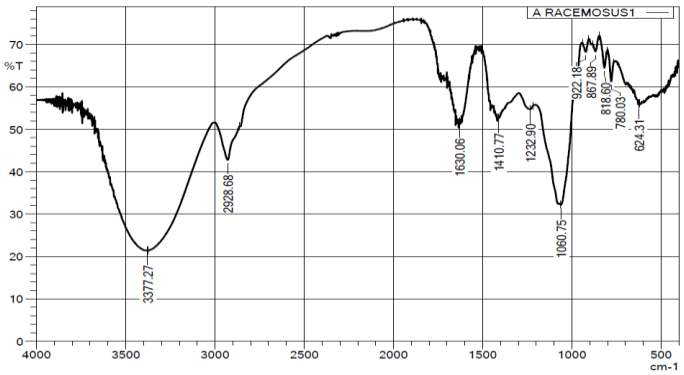

Fig. 14: FTIR spectra of BCAR

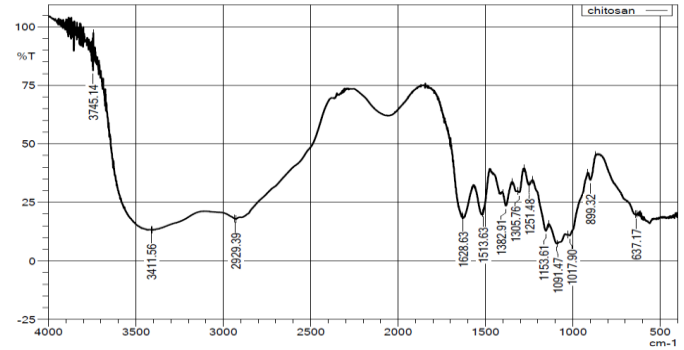

Fig. 15: FTIR spectra of Chitosan

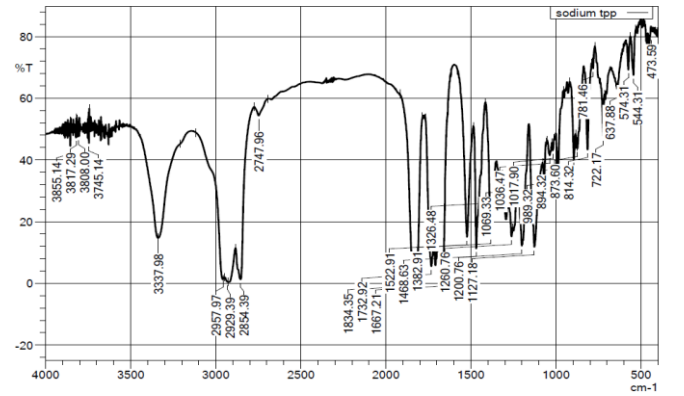

Fig. 16: FTIR spectra of NaTPP

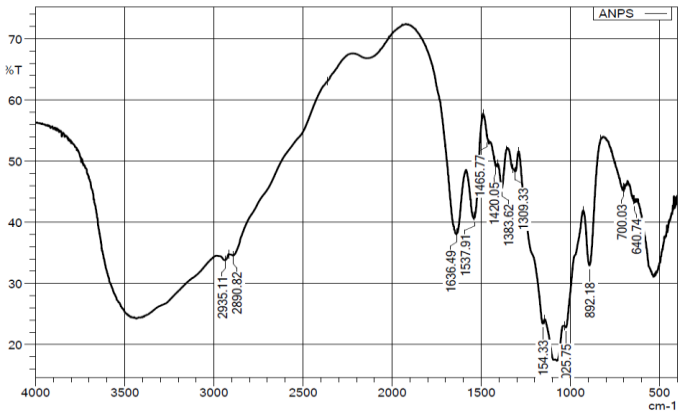

Fig. 17: FTIR spectra of OBCARNP

XRD studies

XRD analysis indicated the amorphous nature of BCAR, the slightly crystalline nature of chitosan, and the crystalline nature of blank nanoparticles and optimized nanoparticles (fig. 18-21).

Particle size

Particle size measurements were required to confirm the formation of nano-range particles. The frequency (percent/nm) on the Y-axis vs diameter (nm) on the x-axis was reported in the particle size distribution spectra for optimized chitosan nanoparticles. The hydrodynamic diameter of the hydrosol was examined using the dynamic light scattering method (particle suspension). The OBCBANPs particle size was determined to be 48.8 nm, as shown in fig. 22. The findings demonstrated the particles' nanoscale size, which is critical in the production of nanoparticles.

Zeta potential

The formulation is stabilized by the zeta potential, an electrical charge on the particle surface that acts as a repulsive force. The optimized chitosan nanoparticle zeta potential spectra were captured as zeta potential versus intensity spectra, with intensity (a. u.) on the y-axis and zeta potential (mV) on the x-axis. The DLS technique was utilized to investigate the hydrosol zeta potential (particle suspension). Strong negative or positive zeta potential hydrosols strive to reject one another, limiting the possibilities of particle aggregation. Furthermore, there won't be any pressure to prevent the particles from adhering to one another and flocculating if the zeta potential values of the particles are weak.

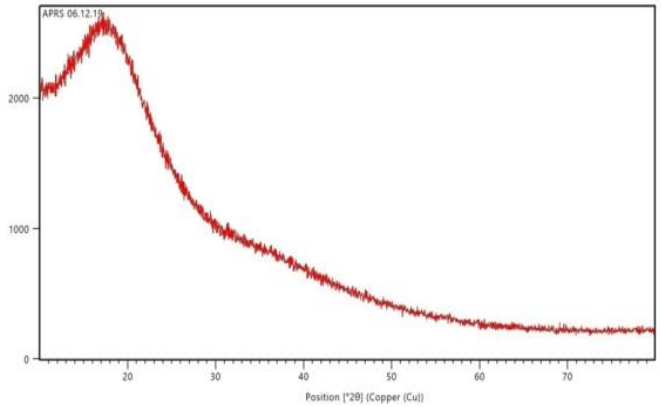

Fig. 18: XRD of BCAR

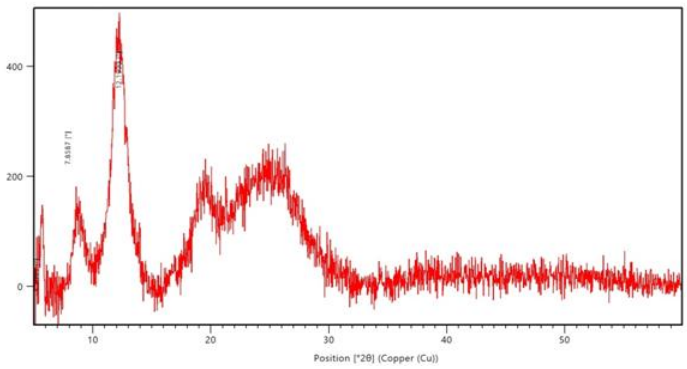

Fig. 19: XRD of chitosan

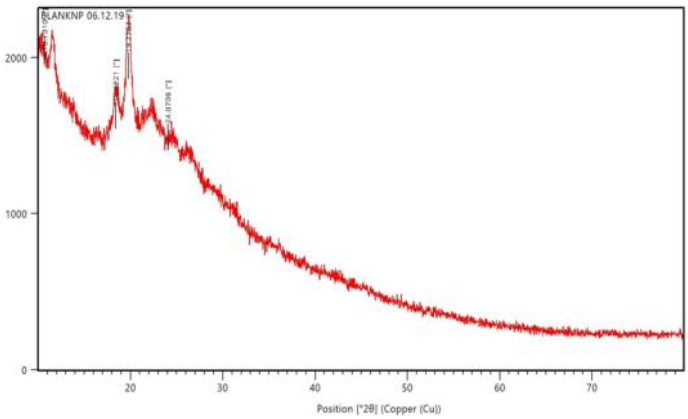

Fig. 20: XRD of blank nanoparticles

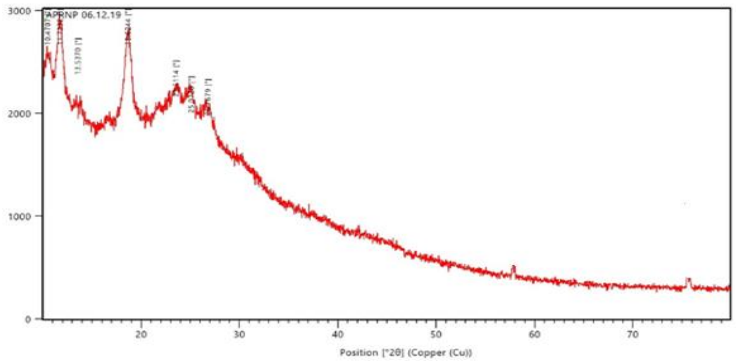

Fig. 21: XRD of OBCARNPs

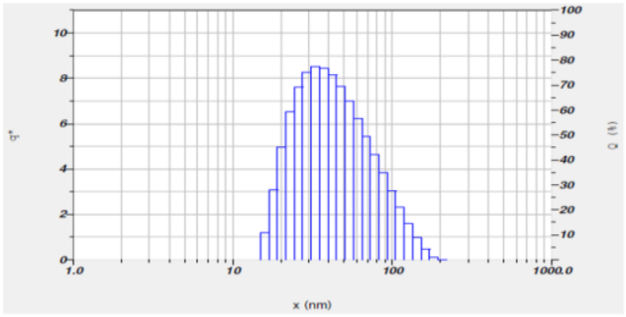

Calculation Results

Peak No.	S.P.Area Ratio	Mean	S. D.	Mode
1	1.00	48.8 nm	28.2 nm	33.0 nm
2	—	-- nm	-- nm	-- nm
3	—	-- nm	-- nm	-- nm
Total	1.00	48.8 nm	28.2 nm	33.0 nm

Fig. 22: Particle size of OBCARNPs

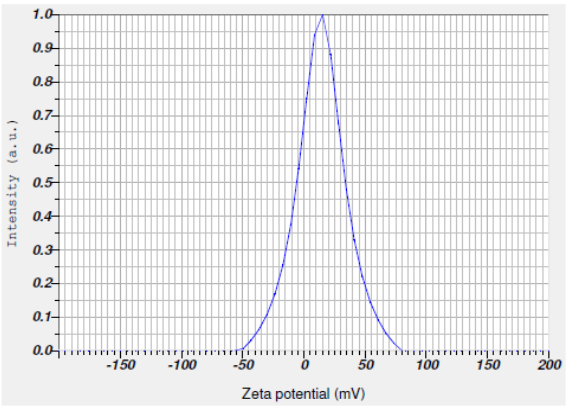

Calculation Results

Peak No.	Zeta Potential	Electrophoretic Mobility
1	14.1 mV	0.000110 cm2/Vs
2	-- mV	-- cm2/Vs
3	-- mV	-- cm2/Vs

Zeta Potential (Mean) : 14.1 mV
Electrophoretic Mobility mean : 0.000110 cm²/Vs

Fig. 23: Zeta potential of OBCARNPs

The zeta potential value of 14.1 mV was found to be positive, implying that the synthesized OBACBANPs had greater stability by inhibiting particle aggregation, as shown in fig. 23. The positive zeta potential value might be attributed to Chitosan's cationic structure and the presence of residual amino groups that are not neutralized by interactions with NaTPP molecules discussed in previous research works. Such amino groups are resistant to anion adsorption and have a high electrical double-layer thickness, resulting in healthy nanoparticles.

Scanning electron microscopy (SEM)

The surface morphology of OBCBANPs viewed in SEM images turns out to be spherical in form with a homogeneous distribution, as shown in fig. 24. The OBCBANPS exhibited low aggregation, a somewhat rough surface, and a mean diameter below 100 nm, according to SEM analysis. A sufficient zeta potential of the particle for repelling the suggested potential stabilization of the

nanoparticles is directly responsible for the lowest possible aggregation, proved in earlier works [26].

Transmission electron microscopy (TEM)

According to TEM images shown in fig. 25, the OBCBANPs employed in this study had a mean diameter of less than 100 nm. Formed OBCBANPs are observed to be spherical in form and tend to be partially aggregated.

Stability testing of OBCARNPs

OBCBANPs were subjected to accelerated stability testing, and the results are tabulated below.

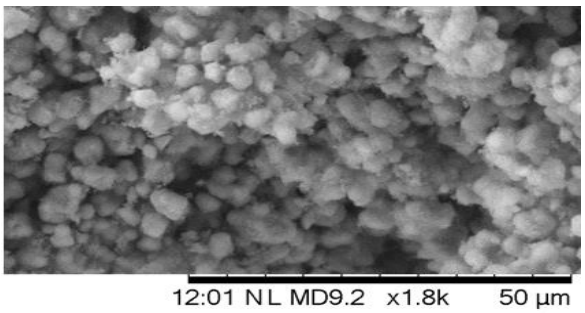

Fig. 24: SEM of OBCARNPs

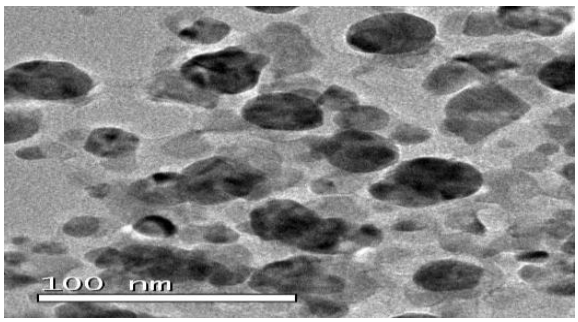

Fig. 25: TEM of OBCARNPs

Table 8: Physical appearance of optimized OBCARNPs during stability studies

Physical appearance of optimized OBCARNPs					
Accelerated conditions	**Formulation**	**15 d**	**30 d**	**60 d**	**90 d**
25 °C/60% RH		Intact	Intact	Intact	Intact
45 °C/65% RH	OBCARNPs	Intact	Intact	Intact	Intact
60 °C/75% RH		Intact	Intact	Intact	Intact

Table 9: % Drug release data of OBCARNPs during stability studies

% Drug release of OBCARNPs (mean±SD; n=3)				
Time (H)	**Formulation**	**15 d**		
		25 °C/60% RH	45 °C/65% RH	60 °C/75% RH
0.5		15.8±0.57	15.1±1.78	16.5±2.23
1		18.6±1.46	19.2±0.96	17.9±1.75
2		25.9±1.67	23.9±0.43	24.8±1.07
4	OBCARNPs	29.8±1.74	30.3±0.65	29.5±2.95
6		34.1±2.56	35.4±1.67	33.9±0.87
8		37.3±0.67	38.9±1.93	39.4±1.03
12		57.3±1.27	59.2±1.25	58.1±0.46
24		78.8±1.87	79.8±0.92	78.3±0.65
		30 d		
		25 °C/60% RH	45 °C/65% RH	60 °C/75% RH
0.5		14.8±0.74	15.8±1.84	15.3±0.47
1		18.9±1.68	19.2±0.87	18.1±2.17
2		24.2±1.92	24.9±3.18	23.9±1.38
4		29.3±0.79	30.1±1.92	30.8±2.18
6	OBCARNPs	34.1±1.78	33.3±0.76	34.8±1.45
8		39.8±0.78	38.9±3.37	39.6±1.78
12		58.1±1.86	58.8±0.97	59.7±2.96
24		79.8±1.71	78.1±1.82	78.2±1.68

% Drug release of OBCARNPs (mean±SD; n=3)				
Time (H)	**Formulation**	**15 d**		
		60 d		
		25 °C/60% RH	45 °C/65% RH	60 °C/75% RH
0.5		16.1±1.37	15.7±0.74	14.7±2.63
1		18.7±1.79	19.2±0.57	19.7±1.64
2		24.9±1.69	23.8±0.84	24.6±3.57
4	OBCARNPs	29.8±0.97	28.9±1.53	30.3±2.74
6		34.8±1.82	33.8±0.67	34.9±0.89
8		39.7±2.47	38.2±0.98	38.5±1.63
12		59.3±1.78	58.4±2.56	59.7±1.87
24		79.4±0.89	79.9±1.86	79.1±1.91
		90 d		
		25 °C/60% RH	45 °C/65% RH	60 °C/75% RH
0.5		15.8±1.76	16.4±0.68	15.5±1.85
1		19.1±2.84	18.3±0.74	19.6±1.73
2		24.7±0.98	23.9±0.74	24.1±2.34
4	OBCARNPs	30.8±1.79	31.4±0.79	28.8±2.96
6		34.9±1.75	33.9±1.67	34.2±2.43
8		39.4±1.37	37.9±1.57	38.9±0.75
12		58.5±0.97	59.4±1.79	58.7±2.81
24		79.8±1.83	78.5±0.45	78.9±1.67

Results mentioned are mean±SD; n=3.

Stability testing of the optimized nanoparticles was performed at different conditions (25 °C/60% RH, 45 °C/65% RH, and 60 °C/75% RH) for 15, 30, 60, and 90 d. The results showed no significant changes in appearance and percent drug release, indicating that the optimized nanoparticles were stable over the tested period.

CONCLUSION

The ionic gelation method is employed in the preparation of BCARNPs. BBD is practiced to achieve desired experimental runs for optimization to cut short the wide range of experimental runs. The regression coefficients established by the second-order polynomial equations of all the responses indicated that the model is significant. Diagnostic plots showed that the quadratic model generated was well matched to all aspects of the experimental design. BCARNPs were optimized with the numerical optimization technique. FTIR studies revealed compatibility among the drug and excipients; XRD studies stated the crystalline nature of nanoparticles due to the gelation of chitosan and NaTPP. The particle size of the optimized formulation was substantiating that the nanoparticles are in the nanorange. The zeta potential inferred the superlative stability of optimized formulation nanoparticles. SEM and TEM analyses illustrated that optimized nanoparticles are spherical in form and homogeneous with minimum aggregation. Accelerated stability studies performed on the optimized formulation stated that there was no substantial variation in appearance and % DR. The presence of glucosamine groups in chitosan serves as a ligand for the megalin receptors associated with renal tubular epithelial cells. Therefore, stable optimized nanoparticles further need to be investigated and established for antiurolithiatic activity by targeting the kidney by performing *in vivo* studies.

ACKNOWLEDGEMENT

The first author expresses deep gratitude to the management and Dr. D. Ranganayakulu, M. Pharm., Ph. D., Professor and Principal of Sri Padmavathi School of Pharmacy, Tiruchanoor, Andhra Pradesh, India, for their support and provision of laboratory facilities.

FUNDING

Nil

AUTHORS CONTRIBUTIONS

The study's scientific contributions encompassed a collaborative effort from all authors. Bhargavi Posinasetty played a key role in collecting and analyzing the data. Srividya Kommineni focused on the nanoencapsulation studies, while Kishore Bandarapalle, Syed Naziya, Daruri Seemantini, and Chanambatla Yamini were involved in various aspects such as literature review, material collection, methodology, and data collection. K. K. Rajasekhar took charge of the characterization study analysis. The culmination of these efforts resulted in the collaborative writing of the final manuscript, with each author contributing their expertise to the research project.

CONFLICTS OF INTERESTS

Declared none

REFERENCES

1. Kumari A, Yadav SK, Yadav SC. Biodegradable polymeric nanoparticles based drug delivery systems. Colloids Surf B Biointerfaces. 2010;75(1):1-18. doi: 10.1016/j.colsurfb.2009.09.001, PMID 19782542.
2. Tønnesen HH, Karlsen J. Alginate in drug delivery systems. Drug Dev Ind Pharm. 2002;28(6):621-30. doi: 10.1081/ddc-120003853, PMID 12149954.
3. Asgharian S, Lorigooini Z, Rafieian R, Rafieian Kopaei M, Kheiri S, Nasri H. The preventive effect of berberis vulgaris extract on contrast-induced acute kidney injury. J Nephropathol. 2017;6(4):395-8. doi: 10.15171/jnp.2017.65.
4. Balaji LG, Banji D, Banji JF. Evaluation of antiurolithiatic activity of the aqueous and alcoholic extracts of roots of *boerhaavia diffusa*. Indo Am J Pharm Res. 2015;5(1):525-30. doi: 10.1044/1980-iajpr.150115.
5. Geng X, Zhang M, Lai X, Tan L, Liu J, Yu M. Small-sized cationic miRi-PCNPs selectively target the kidneys for high-efficiency antifibrosis treatment. Adv Healthc Mater. 2018;7(21):e1800558. doi: 10.1002/adhm.201800558, PMID 30277665.
6. Wang J, Masehi Lano JJ, Chung EJ. Peptide and antibody ligands for renal targeting: nanomedicine strategies for kidney disease. Biomater Sci. 2017;5(8):1450-9. doi: 10.1039/c7bm00271h, PMID 28516997.
7. Gao S, Hein S, Dagnæs Hansen F, Weyer K, Yang C, Nielsen R. Megalin-mediated specific uptake of chitosan/siRNA nanoparticles in mouse kidney proximal tubule epithelial cells enables AQP1 gene silencing. Theranostics. 2014;4(10):1039-51. doi: 10.7150/thno.7866, PMID 25157280.
8. Qiao H, Sun M, Su Z, Xie Y, Chen M, Zong L. Kidney-specific drug delivery system for renal fibrosis based on coordination-driven assembly of catechol-derived chitosan. Biomaterials Biomaterials. 2014;35(25):7157-71. doi: 10.1016/j.biomaterials.2014.04.106.
9. El-ASSAL MI, Samuel D. Optimization of rivastigmine chitosan nanoparticles for neurodegenerative alzheimer; *in vitro* and ex vivo characterizations. Int J Pharm Pharm Sci. 2022;14(1):17-27. doi: 10.22159/ijpps.2022v14i1.43145.

10. Yuan ZX, Zhang ZR, Zhu D, Sun X, Gong T, Liu J. Specific renal uptake of randomly 50% N-acetylated low molecular weight chitosan. Mol Pharm. 2009;6(1):305-14. doi: 10.1021/mp800078a, PMID 19035784.
11. Patel M, Patel NV, Patel TB. Design and development of rilpivirine nanoparticle containing chitosan using ionic gelation method for hiv infections. Int J Pharm Pharm Sci. 2020;12(2):113-8. doi: 10.22159/ijpps.2020v12i2.35814.
12. Vozza G, Danish M, Byrne HJ, Frias JM, Ryan SM. Application of box-Behnken experimental design for the formulation and optimisation of selenomethionine-loaded chitosan nanoparticles coated with zein for oral delivery. Int J Pharm. 2018;551(1-2):257-69. doi: 10.1016/j.ijpharm.2018.08.050, PMID 30153488.
13. Ghose D, Patra CN, Swain S, Sruti J. Box-Behnken design-based development and characterization of polymeric freeze-dried nanoparticles of isradipine for improved oral bioavailability. Int J App Pharm. 2023;15(4):60-70. doi: 10.22159/ijap.2023v15i4.47728.
14. Mao CF, Zhang XR, Johnson A, He JL, Kong ZL. Modulation of diabetes mellitus-induced male rat reproductive dysfunction with micro-nanoencapsulated echinacea purpurea ethanol extract. BioMed Res Int. 2018;2018:4237354. doi: 10.1155/2018/4237354, PMID 30246020.
15. Abo-Elseoud WS, Hassan ML, Sabaa MW, Basha M, Hassan EA, Fadel SM. Chitosan nanoparticles/cellulose nanocrystals nanocomposites as a carrier system for the controlled release of repaglinide. Int J Biol Macromol. 2018;111:604-13. doi: 10.1016/j.ijbiomac.2018.01.044, PMID 29325745.
16. Padmaa PM, Preethy AJ, Setty CM, Peter GCV. Release kinetics–concepts and applications. IJPRT. 2018;8(1):12-20.
17. Fu Y, Kao WJ. Drug release kinetics and transport mechanisms of non-degradable and degradable polymeric delivery systems. Expert Opin Drug Deliv. 2010;7(4):429-44. doi: 10.1517/17425241003602259, PMID 20331353.
18. Ruhi R, Sarika W, Vinay S, Ram G. Pramipexole dihydrochloride loaded chitosan nanoparticles for nose to brain delivery: development, characterization and *in vivo* anti-Parkinson activity. Int J Biol Macromol. 2018;1(109):27-35. doi: 10.1016/j.ijbiomac.2017.12.056.
19. Sonali BS, Bharate SB, Bajaj AN. Interactions and incompatibilities of pharmaceutical excipients with active pharmaceutical ingredients, a comprehensive review. J Excipients Food Chem. 2010;1(3):3-25.
20. Sharma R, Yasir M, Bhaskar S, Asif M. Formulation and evaluation of paclitaxel loaded PSA-PEG nanoparticles. J Appl Pharm Sci. 2011;1(5):96-8.
21. Gannu R, Palem CR, Yamsani SK, Yamsani VV, Yamsani MR. Enhanced bioavailability of buspirone from the reservoir-based transdermal therapeutic system, optimization of formulation employing box–behnken statistical design. AAPS PharmSciTech. 2010;11(2):976-85. doi: 10.1208/s12249-010-9451-7, PMID 20517714.
22. Abul Kalam M, Khan AA, Khan S, Almalik A, Alshamsan A. Optimizing indomethacin-loaded chitosan nanoparticle size, encapsulation, and release using box-Behnken experimental design. Int J Biol Macromol. 2016;87:329-40. doi: 10.1016/j.ijbiomac.2016.02.033, PMID 26893052.
23. Meng J, Sturgis TF, Youan BB. Engineering tenofovir-loaded chitosan nanoparticles to maximize microbicide mucoadhesion. Eur J Pharm Sci. 2011;44(1-2):57-67. doi: 10.1016/j.ejps.2011.06.007, PMID 21704704.
24. Solanki AB, Parikh JR, Parikh RH. Formulation and optimization of piroxicam proniosomes by 3-factor, 3-level box-behnken design. AAPS PharmSciTech. 2007;8(4):E86. doi: 10.1208/pt0804086, PMID 18181547.
25. Gannu R, Palem CR, Yamsani SK, Yamsani VV, Yamsani MR. Enhanced bioavailability of buspirone from the reservoir-based transdermal therapeutic system, optimization of formulation employing box–behnken statistical design. AAPS PharmSciTech. 2010;11(2):976-85. doi: 10.1208/s12249-010-9451-7, PMID 20517714.
26. Rukmangathen R, Yallamalli IM, Yalavarthi PR. Formulation and biopharmaceutical evaluation of risperidone-loaded chitosan nanoparticles for intranasal delivery. Drug Dev Ind Pharm. 2019;45(8):1342-50. doi: 10.1080/03639045.2019.1619759, PMID 31094571.